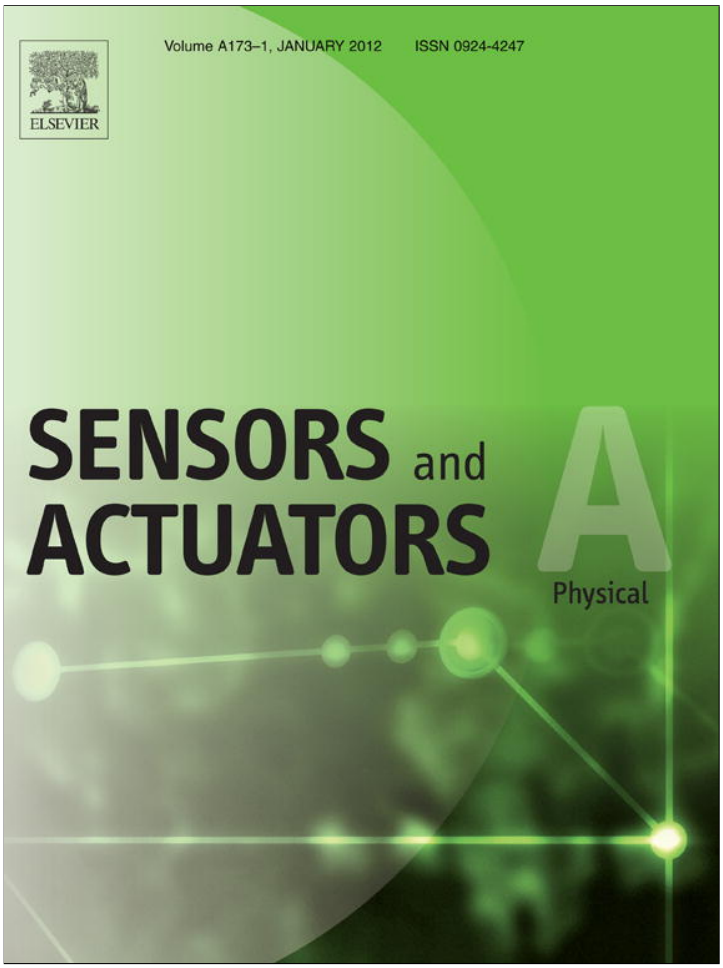

Sensors and Actuators A 173 (2012) 190–196

Contents lists available at SciVerse ScienceDirect

Sensors and Actuators A: Physical

journal homepage: www.elsevier.com/locate/sna

Enhancing displacement of lead–zirconate–titanate (PZT) thin-film membrane microactuators via a dual electrode design

Chuan Luo [a], G.Z. Cao [b], I.Y. Shen [a,*]

[a] Department of Mechanical Engineering, University of Washington, Seattle, WA 98195-2600, USA
[b] Department of Material Science & Engineering, University of Washington, Seattle, WA 98195-2120, USA

ARTICLE INFO

Article history:
Received 25 May 2011
Received in revised form 11 October 2011
Accepted 21 October 2011
Available online 25 October 2011

Keywords:
PZT thin films
Micro-actuators
Dual electrodes
Finite element analyses

ABSTRACT

A common design of piezoelectric microactuators adopts a membrane structure that consists of a base silicon diaphragm, a layer of bottom electrode, a layer of piezoelectric thin film, and a layer of top electrode. In particular, the piezoelectric thin film is often made of lead–zirconate–titanate (PZT) for its high piezoelectric constants. When driven electrically, the PZT thin film extends or contracts flexing the membrane and generating an out-of-plane displacement. Many manufacturing defects, however, could significantly reduce the designed actuator displacement. Examples include residual stresses, warping, non-uniform etching of the silicon diaphragm, and misalignment between the top electrode and the silicon diaphragm. The purpose of this paper is to develop a dual top-electrode design to enhance the actuator displacement. In this design, the top electrode consists of two disconnected (thus independent) electrode areas, while a continuous bottom electrode serves as the ground. The two top electrodes are located in two regions with opposite curvature when the diaphragm deflects. When the two top electrodes are driven in an out-of-phase manner, the actuator displacement is enhanced. Finite element analyses and experimental measurements both confirm the feasibility of this design. When manufacturing defects are present, experimental results indicate that the actuator displacement can be optimized by adjusting the phase difference between the dual top electrodes.

1. Introduction

Lead–zirconate–titanate (PZT) thin-film microactuators often take the form of a membrane structure. Such membrane actuators typically consist of four parts: a diaphragm, a bulk silicon substrate, a PZT thin film layer, and a pair of electrodes, see Fig. 1. (Note that the parts in Fig. 1 are not drawn in proportion.) The diaphragm is a moving component of the actuator anchored to the silicon substrate. As a result of its small thickness, the silicon diaphragm has low structural stiffness compared with the substrate. On top of the silicon diaphragm is a layer of PZT thin film with a pair of bottom and top electrodes. When a driving voltage is applied to the electrodes, the PZT thin film extends or contracts in the plane of the diaphragm, thus creating a bending moment to flex the diaphragm out of its plane. Such PZT thin-film membrane actuators have appeared in many applications including micro fluidic devices (pumps and valves [1], nozzles [2]), micro scanners [3], micro-deformable mirrors [4,5], micro high fidelity speakers [6,7], micro protein desorption device [8], hybrid cochlear implant actuators [9], fuel cell membrane [10]. In addition, similar structure are also widely used in various transducers, such as micro energy generators [11,12], micro mass sensing devices [13,14], ultrasonic transducers [15], acoustic transducers [16], and micro pressure sensors [17].

For many applications, it is important to maximize the actuator constant, which is defined as the displacement generated per unit voltage applied. For example, microactuators to generate acoustic pressure waves in intracochlear applications have a specification of 200 nm in displacement. If the actuator constant is large, only a small voltage is needed to drive the actuator to achieve the desire displacement.

In fabricating the PZT thin-film microactuators, there are many factors that could significantly reduce the actuator constant from its designed value. For example, residual stresses are unavoidable during the fabrication, because high sintering temperature of PZT thin films together with a tiny mismatch of coefficient of thermal expansion can result in huge residual stresses in the actuator [18–22]. The presence of the residual stresses will significantly stiffen the diaphragm and reduce the actuator constant. As another example, the diaphragm is often fabricated by etching away part of the bulk silicon substrate from the bottom. The etching is seldom uniform resulting in residual silicon at the junction of the diaphragm

* Corresponding author. Tel.: +1 206 543 5718; fax: +1 206 685 8047.
E-mail address: ishen@u.washington.edu (I.Y. Shen).

0924-4247/$ – see front matter © 2011 Elsevier B.V. All rights reserved.
doi:10.1016/j.sna.2011.10.022

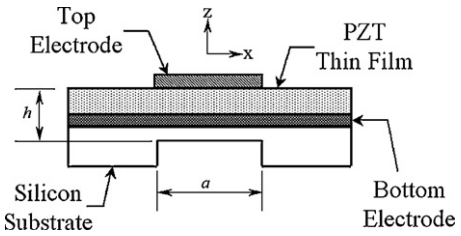

Fig. 1. Schematic drawing of PZT thin-film membrane actuator (not to scale).

and the silicon substrate [18]. The residual silicon increases the diaphragm thickness and stiffens the actuator thus reducing the actuator constant.

To increase the actuator constant, the current practice is to optimize relative size of the top electrode to the residual silicon [18]. Both simulation and experimental results indicate that the actuator constant reaches its maximum when the size of the top electrode is roughly 60% of the size of the residual silicon. This design, however, has several drawbacks. First, this design has only one top electrode spanning partially over the diaphragm structure. Therefore, the real estate of the actuator is not fully utilized to increase the actuator constant. Second, the top electrode is optimized with respect to the residual silicon, which may vary from batch to batch depending on fabrication conditions. Therefore, the design is somewhat "passive" and lacks flexibility in adapting to various fabrication conditions.

Fig. 2 shows the normal strain in the *x* direction of the passive silicon membrane from a finite element analysis for a single-electrode design (cf. Fig. 1). The strain distribution consists of two regions. The first region is the central region covered by the top electrode. In this region, the silicon experiences positive strain, indicating that the diaphragm is extended. Since the deformation under the top electrode comes from the piezoelectric effect, this part of diaphragm can be termed as "active diaphragm." The second region is outside the top electrode, and it experiences a uniform negative strain and hence contraction. For a single electrode design, the PZT thin film in this outside region not only fails to contribute any actuation, but also increases stiffness of the diaphragm reducing the actuator displacement. In a sense, the second region is a "passive diaphragm" for a single-electrode design.

Motivated by this observation, this paper is to develop a dual top-electrode design to significantly increase the actuator constant. In this design, the top electrode consists of two disconnected (thus independent) electrode areas, while a continuous bottom electrode serves as the ground. The basic idea is the following. As indicated in Fig. 2, the diaphragm deforms into two concentric areas whose

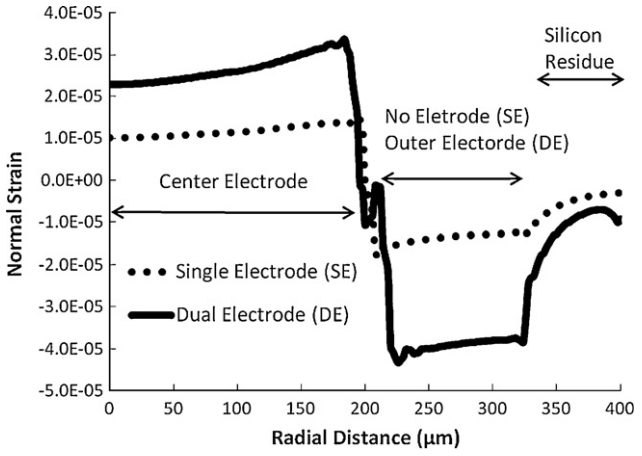

Fig. 2. Comparison of normal strain in the radial direction at the top surface of the passive silicon.

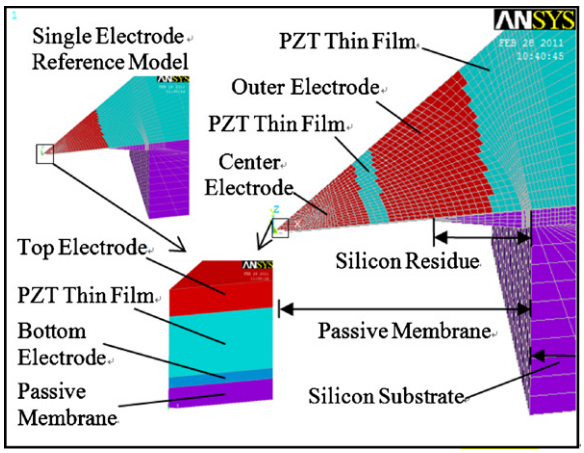

Fig. 3. Finite element models.

curvatures are opposite. (For example, one is concave upward and the other is concave downward.) Therefore, a second electrode in the passive region will turn it into an active diaphragm as well. When it is driven in an out-of-phase manner to the center electrode, it will significantly enhance the actuator displacement.

This design has two advantages over the single top-electrode design. First, it fully utilizes the real estate of the actuator diaphragm to increase the actuator constant. Second, it can adapt to manufacturing defects (e.g., misalignment between the top electrode and the diaphragm) by adjusting the phase angle between the driving voltages of the two electrodes.

For the rest of the paper, we will first demonstrate the enhancement of actuator constant via a finite element analysis. Then experiments will be conducted to show the feasibility of the dual top-electrode design. Two additional cases are presented to demonstrate the versatility of this design. One is misalignment between the top electrode and the silicon diaphragm. The other is the effect of warping of the actuator diaphragm.

2. Finite elements analysis

2.1. Model development

To study the displacement enhancement produced by the dual electrodes design, two finite element models are created using ANSYS. One is a reference model with a single top electrode, while the other has dual top electrodes for comparison.

The reference model is described in [18], which is a one-eighth model of the actuator; see the top left part of Fig. 3. The model consists of six components: a silicon substrate, a passive silicon membrane, a silicon residue, a PZT thin film and a pair of top and bottom electrodes (Fig. 3). The silicon substrate has dimensions of 3000 μm × 3000 μm with a thickness of 400 μm. At the center of the substrate, a silicon block of 800 μm × 800 μm is removed to form the passive membrane with a thickness of 0.4 μm.

The silicon residue is located below the passive silicon membrane; see Fig. 3. The silicon residue has a circular inner circumference and a square outer circumference. The inner diameter of the silicon residue varies from 500 μm to 700 μm depending on fabrication conditions. Moreover, the cross section of the silicon residue is trapezoidal with a constant slope angle measured from the SEM photo [18]. As a result, shape and volume of the silicon residue can be completely defined through the inner diameter. The nodes of the silicon residue are merged with the bottom surface of the passive silicon membrane and the inner circumference of the silicon substrate.

The silicon substrate, passive silicon membrane and silicon residue are all meshed with 3D linearly elastic solid elements. The bottom surface of the silicon substrate is subjected to geometrically fixed boundary conditions.

On top of the passive silicon membrane there is a PZT thin film sandwiched between a bottom electrode and a top electrode. In addition, the bottom surface of the bottom electrode is fixed to the top surface of the passive membrane; see Fig. 3. The PZT thin film, top electrode and bottom electrode has a thickness of 1 μm, 0.2 μm and 0.5 μm, respectively. The PZT thin film and the bottom electrode span the entire top surface of the actuator, whereas the top electrode occupies an area of 400 μm × 400 μm at the center of the passive membrane (on the top surface of the PZT thin film).

The PZT thin film is meshed with 3D coupled field solid elements that couple electric, piezoelectric, and structural fields. The electrical potential of the nodes interfacing the top electrode is coupled together. A constant voltage is applied to serve as an electrical boundary condition. An identical setup is made for the nodes interfacing the bottom electrode. Material properties of bulk PZT (PZT-4) are assumed, because exact material properties of PZT thin films remain unknown and could depend significantly on the fabrication process and quality of the films.

The top and bottom electrode are meshed with 3D linear elastic solid elements (i.e., same as the silicon substrate and passive membrane). The nodes at the interfaces of PZT thin film and electrodes are merged together, and so are the nodes at the interface between the bottom electrode and the passive membrane. It is not necessary to consider electrodynamics within the electrodes, because the electrodes will reach an electric equilibrium much faster than the actuator reaches a mechanical equilibrium. Therefore, only the mechanical properties of the two electrodes are needed in the model.

A linear static analysis is then conducted to predict the deflection of the passive membrane. Since the lowest natural frequency of this finite element model is above 50 kHz, harmonic response of the actuator substantially below the first natural frequency (e.g., audio frequency range) can be predicted via a static analysis to reduce computational efforts.

Fig. 3 also shows the finite element model with dual top electrodes consisting of a center electrode and an outer electrode. The center electrode is identical to that of the reference model. The outer electrode has a width of 195 μm surrounding the center electrode like a rectangular frame. Between the two electrodes, there is a gap of 20 μm. The two electrodes can be driven independently by prescribing different voltages as electrical boundary conditions. The two top electrodes, however, share the same bottom electrode. Therefore, three electrical potential values will be assigned in the dual-electrode model.

Other features of the dual-electrode model are identical to that of the reference model. For example, the dual-electrode model has the same properties, element types, meshing, and linear static analysis.

2.2. Simulation results

Fig. 4 compares the actuator displacement with single and dual top electrode designs as a function of radial position, where the diameter of the silicon residue is 650 μm. For the single top electrode design, the voltage of the top electrode is 1 V and the bottom electrode is grounded. For the dual top electrode design, the voltage of the center and outer electrodes is 1 V and −1 V, respectively, while the bottom electrode is grounded. The maximal displacement of the single and dual top electrode design occurring at the center is 0.41 μm and 0.54 μm, respectively. The presence of the second electrode increases the maximal actuator displacement by 32%.

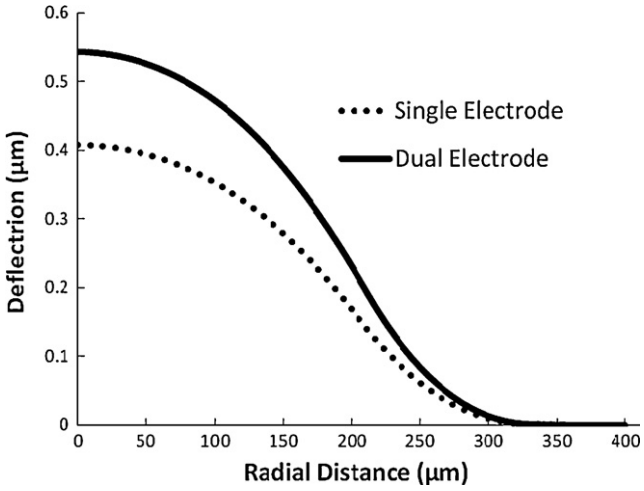

Fig. 4. Comparison of actuator displacement for single and dual top electrode design.

Fig. 2 compares the normal strain σ_x from the dual- and single-electrode designs. The presence of the second top electrode significantly enhances the strain in the regions under both electrodes. As a result, actuator displacement is increased. Fig. 5 shows the normal strain distribution along the thickness (z-direction) of the diaphragm at the center of the actuator. The presence of the second electrode increases the strain throughout the entire thickness.

2.3. Optimization study

With the help of the finite element model, we can conduct simple parametric studies to optimize the geometry of the dual-electrode design to maximize the actuator constant. Fig. 6 shows how actuator displacement (at the center) varies with respect to the size of the center electrode. (The outer electrode has a fixed outer dimension of 800 μm and maintains a 20-μm gap with the center electrode.) The maximal actuator displacement occurs around 320 μm, whereas the residual silicon has a diameter of 650 μm. So the best actuator performance occurs when the size of the center electrode is about half of that of the residual silicon.

Let us consider the case that the center electrode is optimized at 320 μm and the size of the residual silicon is 650 μm. Under these conditions, effects of the size of the outer electrode are studied via the finite element model. Fig. 7 shows how the

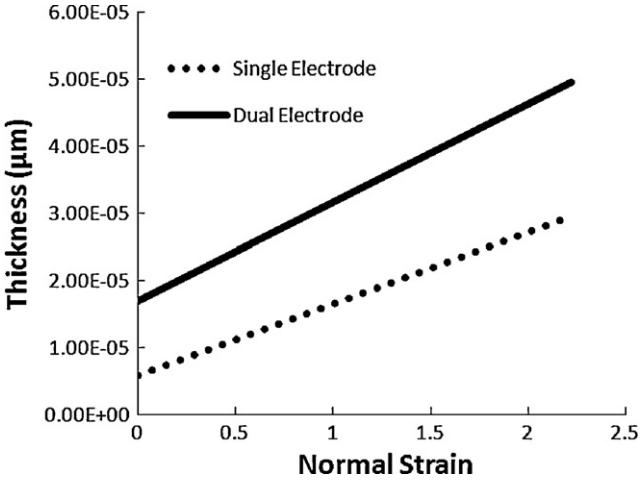

Fig. 5. Comparison of the normal strain along the thickness of the diaphragm.

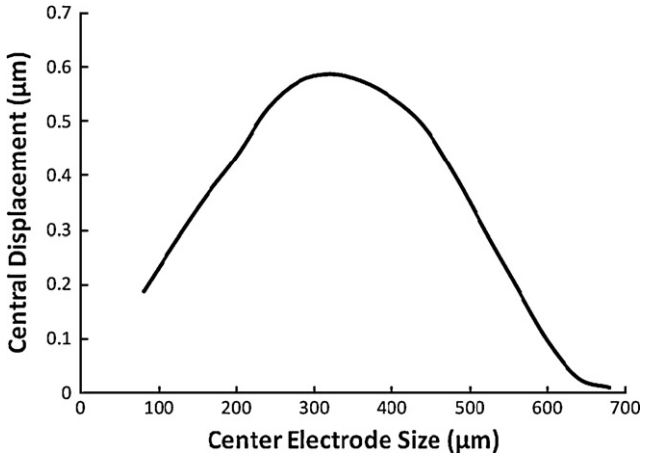

Fig. 6. Actuator displacement with respect to the seize of center electrode.

displacement at the actuator center varies with respect to the size of the outer electrode. The variation consists of three portions. When the outer electrode exceeds 650 μm, the displacement saturates around 0.58 μm. As the outer electrode decreases in size, the displacement drops steadily and stabilizes at 0.4 μm. Since the size of the residual silicon is 650 μm, results from Fig. 7 imply that the outer electrode must overlap with the residual silicon to deliver the maximal actuator displacement.

3. Experimental verification

Calibrated experiments are conducted to verify the simulation results. Specimen preparation, experimental setup and measurement results are described in detail as follows.

3.1. Specimen preparation

Fig. 8 illustrates the fabrication process using an improved sol–gel process that employs rapid thermal annealing and a dilute sealant coating. The silicon substrate is first oxidized in a furnace at 1045 °C for 2 h to grow a SiO_2 layer of 500 nm thick. Then a layer silicon nitride of 200 nm thick is deposited by PECVD (plasma enhanced chemical vapor deposition). The bottom electrode consists of Pt/Ti layers with thickness of 100 nm and 50 nm,

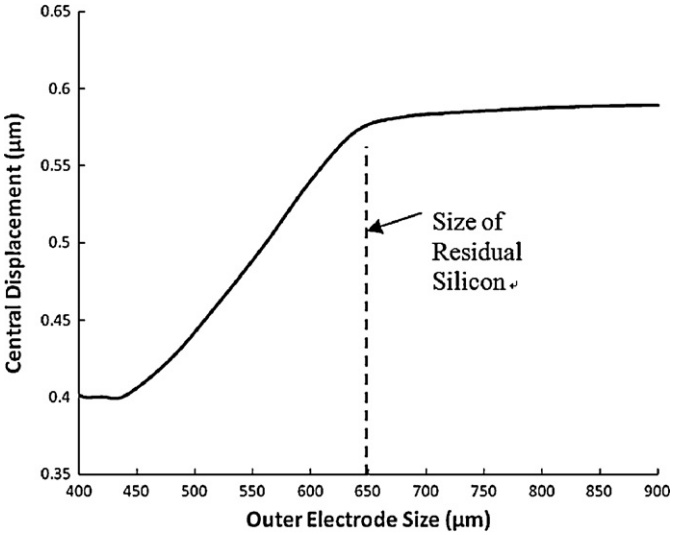

Fig. 7. Actuator displacement with respect to the size of the outer electrode.

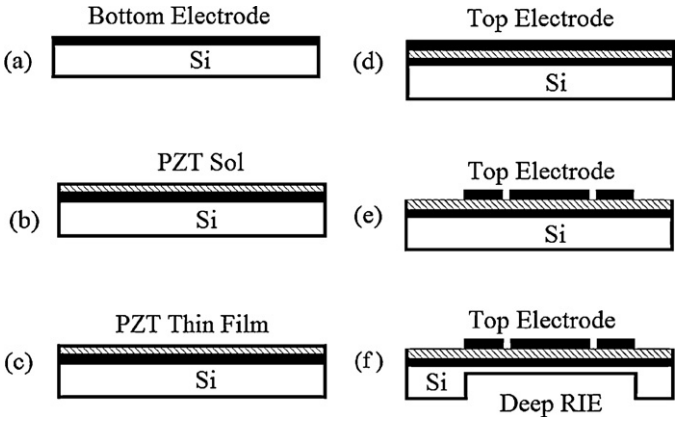

Fig. 8. Preparation processes of actuators.

respectively (Fig. 8(a)). The PZT film is spin-coated three times. For the first two coatings, the sintering temperature is 650 °C for 15 min. For the third coating, the sol is diluted 50% by acetic acid and sintering temperature is 450 °C for 10 min (Fig. 8(b) and (c)). To fabricate the top electrodes, conducting layers consisting of Au/Cr are deposited through evaporation (Fig. 8(d)). The dual top electrodes are patterned and formed through lift-off (Fig. 8(e)). Finally, the backside of the silicon is etched via deep reactive ion etch (DRIE) to form the diaphragm suspension (Fig. 8(f)).

Fig. 9 shows the top view of the fabricated actuator with dual top electrodes under an optical microscope. As one can see, the outer electrode does not completely enclose the center electrode, because space is needed for a connecting wire to reach the center electrode from outside. For the actuator shown in Fig. 9, the center electrode is 390 μm × 390 μm, and the width of the connecting wire is 100 μm. In addition, the outer electrode is 800 μm × 800 μm; therefore, it is the same size as the diaphragm. The circle in dash line refers to the boundary of the residual silicon, which is about 650 μm.

3.2. Experimental setup and results

The experiment setup consists of two function generators, a laser Doppler velocimetry (LDV), an oscilloscope, and an actuator specimen to be tested; see Fig. 10. The function generators drive the center and outer electrode, respectively. The excitations are sinusoidal with a frequency of 3 kHz. Moreover, the phase difference between the two driving voltages is adjustable. The LDV measures

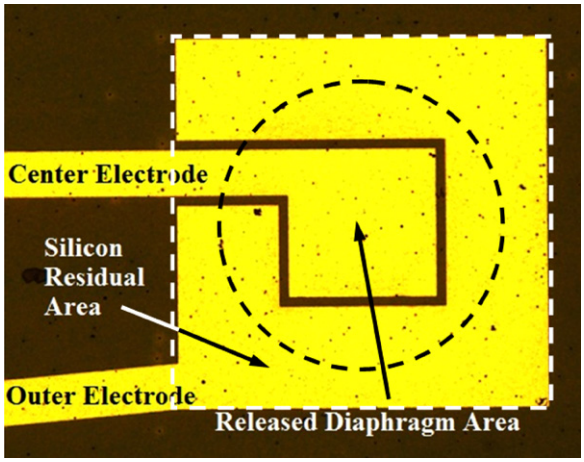

Fig. 9. Microscope picture of the actuator.

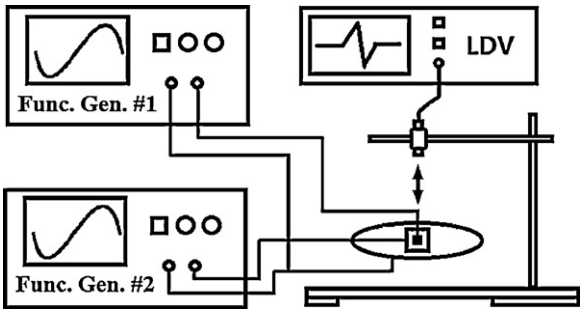

Fig. 10. Schematics of experiment setup.

out-of-plane velocity of the actuator specimen. The oscilloscope records the two input driving signals and the output LDV velocity measurement. In particular, channels 1 and 2 of the oscilloscope represent the driving signal for the center electrode and the outer electrode, respectively. Channel 3 records the LDV velocity measurement.

The measurements of actuator displacements under dual excitations with different phase differences are shown in Fig. 11 as a polar plot. The radial scale shows the measured actuator constant in nm/V, while the circumferential direction indicates the phase difference of the dual excitations in degrees. The actuator displacement reaches its maximum of 17 nm/V when the phase difference is 180°. When the two electrodes are driven in the same phase, the actuator has a minimal displacement of 5 nm/V. A phase difference of 90° generates a median displacement of about 12 nm/V. These results are consistent with those predicted from the finite element analysis.

3.3. Applications to misaligned microactuators

As mentioned above, fabrication defects could significantly decrease performance of the actuator in terms of actuator displacement. One type of defects is misalignment of the top electrode and the diaphragm (and therefore the cavity released via DRIE underneath the diaphragm); see Fig. 12. Such misalignment could decrease the performance of the actuator for two reasons. First, the effective area of the electrode is smaller, because part of top electrode may not be on the released diaphragm. Second, the position

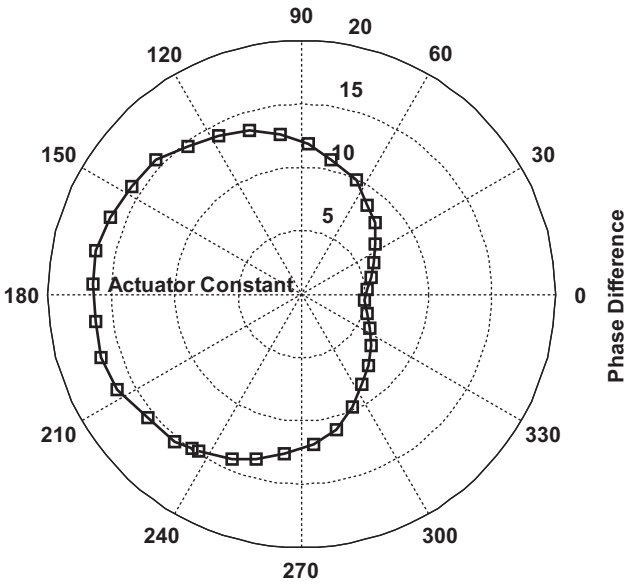

Fig. 11. Displacements under excitation with different phase difference.

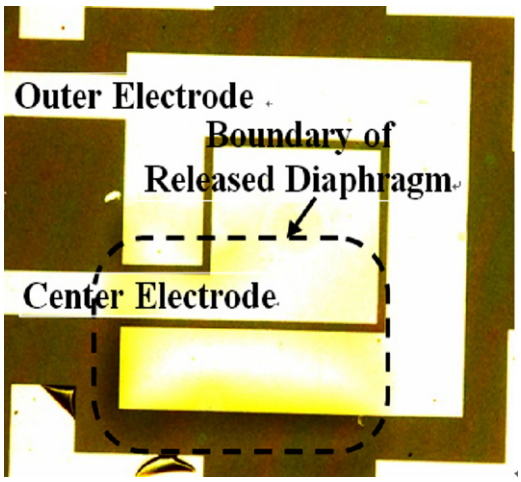

Fig. 12. Microscope picture of the misaligned actuator.

of the top electrode is away from the optimized position (i.e., center of the diaphragm).

The same experimental setup was applied to the misaligned actuator shown in Fig. 12. The driving signals to the center and outer electrodes have the same magnitude, but the phase difference is adjustable. Fig. 13 shows the measured out-of-plane velocity of the actuator in the form of a polar plot. The radial readings are the actuator constant (i.e., displacement per volt in nm/V) and the circumferential readings refer to the phase difference (in degrees). When the phase difference is 14.8°, the actuator has the smallest displacement of 16 nm/V. In contrast, when the phase difference is −172.2°, the actuator has the largest displacement of 29 nm/V.

There are two things worth noting. First, the outer electrode now occupies as large an area of the released diaphragm as the center electrode due to the misalignment. Therefore, activation of the outer electrode can now significantly improve the performance of the actuator. Second, the dual-electrode setup allows flexible adjustment of the phase angle to maximize the actuator displacement. As a result of the misalignment, the maximal displacement does not occur at 180° any more. Since manufacturing defects are unavoidable, the use of dual top electrodes can serve as an effective way to enhance the yield of the manufactured actuators.

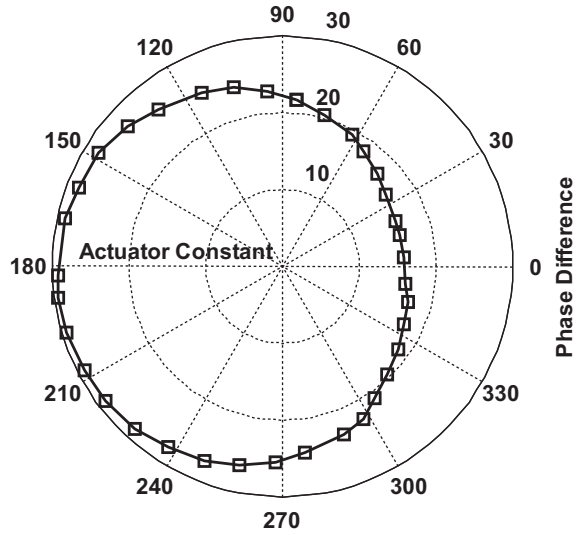

Fig. 13. Displacements under excitation with different phase difference (misaligned actuator).

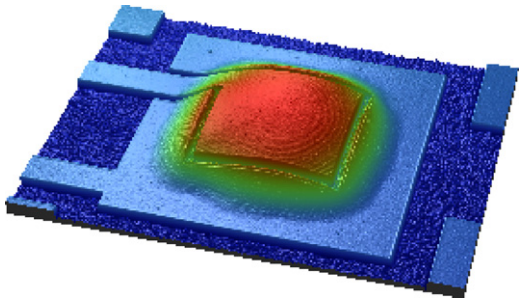

Fig. 14. 3D profile picture of the warped actuator.

3.4. Effects of warping

The finite element analyses above assume that the actuator always has a flat diaphragm. In reality, the diaphragm may warp due to residual stresses resulting from the sintering process of the PZT thin film at elevated temperature. For example, Fig. 14 shows the surface profile measured through an optical profiler NT3300 indicating a bulge of 3.89 μm with the released diaphragm. Naturally, the finite element predictions above may break down when the warping becomes significant.

We have also conducted experiments on warped actuators. The maximum displacement, however, occurs when the center and the outer electrodes are driven in the same phase. As shown in Fig. 15, the two driving voltages (channels 1 and 2) are almost in phase and the resulting actuator velocity measurement (in channel 3) is about 18 mV peak-to-peak. In Fig. 16, the two driving voltages (channels 1 and 2) are almost out of phase and the result velocity measurement is about 8 mV peak-to-peak. This is about 55% reduction from the response under in-phase excitation. The measurement results over 360° shift are shown as a polar plot in Fig. 17.

These experimental results, at first glance, may seem to contradict the finite element predictions. But one needs to realize that there are two components contributing to the out-of-plane displacement of the actuator diaphragm. The first component results from bending of the diaphragm. When the PZT thin film extends or contracts, it generates a bending moment flexing the diaphragm resulting in an out-of-plane displacement. This effect is always present whether or not the actuator diaphragm is warped. Also, the center and outer electrodes must be out of phase in order to maximize this out-of-phase component.

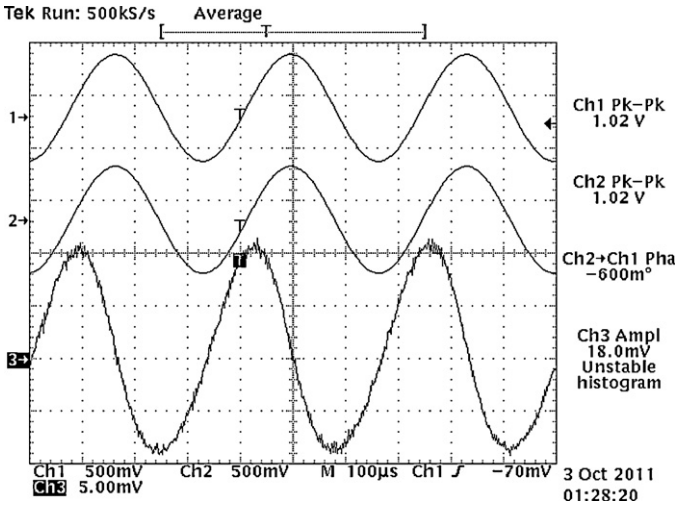

Fig. 15. Actuator excited by both electrodes (in phase).

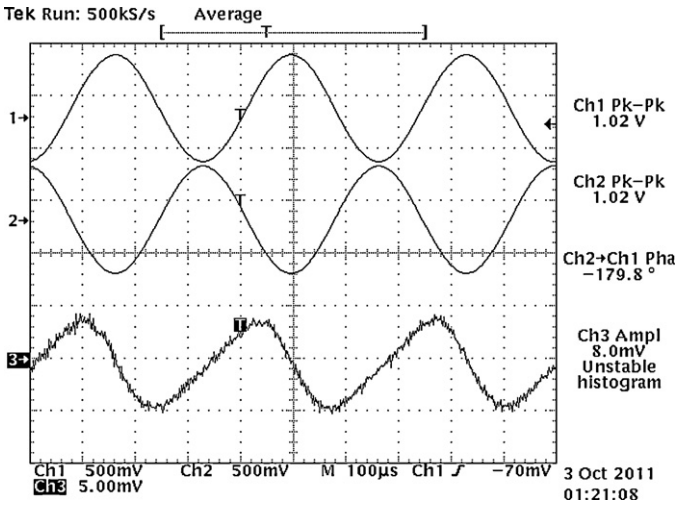

Fig. 16. Actuator excited by both electrodes (out of phase).

In contrast, the second component results from in-plane deformation of the diaphragm. When in-plane deformation occurs, the corresponding in-plane motion takes place along the mid-surface of the diaphragm. When the actuator diaphragm is perfectly flat, the mid-surface is flat. Since the boundary conditions are fixed at four edges, the in-plane motion along the mid-surface cannot change the length of the diaphragm. As a result, the in-plane motion is confined to the flat actuator plane leading to no out-of-plane motion.

When the actuator diaphragm is warped, the mid-surface is no longer flat. In-plane motion along the mid-surface can change the length of the diaphragm and the curvature of the mid-surface (e.g., via bulging or flattening). When this happens, an out-of-plane displacement component occurs simultaneously in order to maintain the fixed boundary conditions at the edges. To maximize this out-of-plane component, the center and outer electrodes should be in the same phase, so that they extend or contract together to increase the change of the diaphragm length.

The competition of these two out-of-plane components will depend on many factors, such as degree of warping, severity of residual stresses, physical dimensions of the remaining silicon, and the thickness of the layers in the actuator diaphragm.

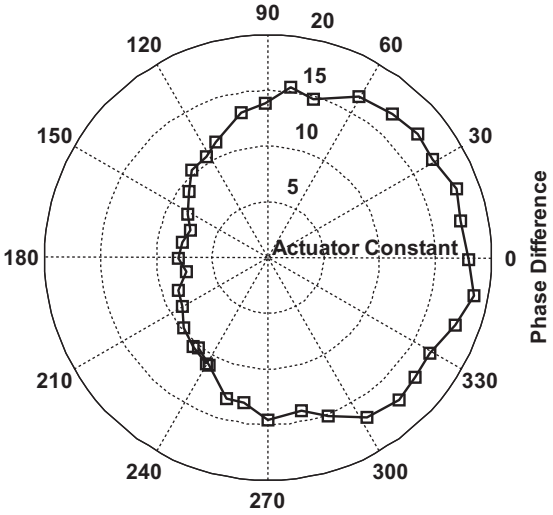

Fig. 17. Displacements under excitation with different phase difference (warped actuator).

4. Conclusions

In this paper, we have demonstrated an effective design to enhance displacement of a PZT thin-film actuator by employing dual top electrodes. The dual-electrode design consists of a center electrode and an outer electrode driven independently. By adjusting the phase angle between the two driving electrodes, one can maximize the actuator displacement. Furthermore, the dual-electrode design can effectively accommodate imperfections from manufacturing, such as misalignment and warping, to meet specifications in displacement and thus increase the yield.

Acknowledgments

This material is based upon work supported by the National Science Foundation under Grant No. CMMI-0826501. Any opinions, findings, and conclusions or recommendations expressed in this material are those of the authors and do not necessarily reflect the views of the National Science Foundation.

References

[1] Y. Luo, M. Lu, T. Cui, A polymer-based bidirectional micropump driven by a PZT bimorph, Microsystem Technologies 17 (40) (2011) 3–409.
[2] J. Akedo, M. Lebedev, Fabrication of microfluidic-devise (diffuser or mixer) using aerosol deposition method, Nano- and Microtechnology: Materials, Processes, Packaging, and Systems 23 (2002) 4–240.
[3] T. Kobayashi, R. Maeda, T. Itoh, Low speed piezoelectric optical microscanner actuated by piezoelectric microcantilevers using $LaNiO_3$ buffered $Pb(Zr,Ti)O_3$ thin film, Smart Materials and Structures 18 (2009).
[4] E.J. Ruggiero, D.J. Inman, Modeling and control of a 2-d membrane mirror with a PZT bimorph, International Mechanical Engineering Congress and Exposition (2006).
[5] Y. Hishinuma, E. Yang, Piezoelectric unimorph microactuator arrays for single-crystal silicon continuous-membrane deformable mirror, Journal of Microelectromechanical Systems 15 (37) (2006) 0–379.
[6] Y. Choe, S. Chen, E.S. Kim, High fidelity loud microspeaker based on PZT bimorph diaphragm, in: NSTI Nanotechnology Conference and Expo 2, 2010, pp. 316–319.
[7] J. Cho, S. Jang, H. Nam, A piezoelectrically actuated mems speaker with polyimide membrane and thin film pb(zr ti)o3(pzt) actuator, Integrated Ferroelectrics 105 (2) (2009) 7–36.
[8] P.Y. Yeh, Y. Le, J. Kizhakkedathu, M. Chiao, An investigation of vibration-induced protein desorption mechanism using a micromachined membrane and PZT plate, Biomedical Microdevices 10 (70) (2008) 1–708.
[9] C. Lee, C. Hume, G. Cao, I. Shen, A feasibility study of PZT thin-film microactuators for hybrid cochlear implants, in: Proceedings of the 2005 27th Annual International Conference of the Engineering in Medicine and Biology Society, IEEE-EMBS, 2005, pp. 1929–1932.
[10] H. Ma, S. Huang, Y. Cheng, C. Yu, C. Hou, A. Su, Study of proton exchange membrane fuel cells (PZT-PEMFCS) with nozzle and diffuser, in: 7th International Conference on Fuel Cell Science, Engineering, and Technology, Compendex, 2009, pp. 9–15.
[11] M. Changki, L.J. Radziemski, W.W. Clark, Analysis of PMN-PT and PZT circular diaphragm energy harvesters for use in implantable medical devices, Active and Passive Smart Structures and Integrated Systems 6525 (2007) 7–16.
[12] D. Shen, J. Ajitsria, S. Choe, D. Kim, Evaluation and modeling of power generator with bimorph PZT cantilever, MRS Materials Research Society 966 (27) (2006) 5–280.
[13] D. Isarakron, D. Briand, A. Sambri, S. Gariglio, J.M. Triscone, F. Guy, J.W. Reiner, C.H. Ahn, N.F. Derooij, Finite element analysis and experiments on a silicon membrane actuated by an epitaxial PZT thin film for localized-mass sensing applications, Sensors and Actuators, B: Chemical 153 (5) (2011) 4–63.
[14] T. Xu, J. Miao, Y. Liu, C.M. Li, Investigation of the effect of adsorption induced surface stress on the resonant frequency of PZT membrane based biosensors, in: 5th IEEE International Conference on Nano/Micro Engineered and Molecular Systems, NEMS, Compendex, 2010, pp. 569–572.
[15] S. Xiong, H. Kawada, H. Yamanaka, T. Matsushima, P. Muralt, Highly sensitive PZT thin film ultrasonic micro-sensors with grooved diaphragm, in: 16th IEEE International Symposium on the Applications of Ferroelectrics, Compendex, 2007, pp. 707–710.
[16] K. Yamashita, K. Tomiyama, K. Yoshikawa, M. Noda, M. Okuyama, Resonant frequency tuning of piezoelectric ultrasonic microsensors by bias voltage application to extra top-electrodes on PZT diaphragms, Ferroelectrics 408 (4) (2010) 8–54.
[17] V. Mohammadi, M.H. Sheikhi, S. Torkian, A. Barzegar, E. Masumi, S. Mohammadi, Design, modeling and optimization of a piezoelectric pressure sensor based on thin-film PZT diaphragm contain of nanocrystalline powders, in: 6th International Symposium on Mechatronics and its Applications, Compendex, 2009.
[18] C. Lee, Q. Guo, G.Z. Cao, I.Y. Shen, Effect of electrode size and silicon residue on piezoelectric thin-film membrane actuators, Sensors and Actuators A 147 (27) (2008) 9–285.
[19] L. Lian, N.R. Sottos, Stress effects in sol–gel derived ferroelectric thin films, Journal of Applied Physics 95 (January) (2004) 629–634.
[20] S. Corkovic, R. Whatmore, Q. Zhang, Development of residual stress in sol–gel derived $Pb(Zr,Ti)O_3$ films: an experimental study, Journal of Applied Physics 103 (April) (2008) 084101.
[21] S. Sengupta, S. Park, D. Payne, L. Allen, Origins and evolution of stress development in sol–gel derived thin layers and multideposited coatings of lead titanate, Journal of Applied Physics 83 (February) (1998) 22910–32296.
[22] E. Hong, R. Smith, S. Krishnaswamy, C. Freidhoff, S. Trolier-McKinstry, Residual stress development in $Pb(Zr,Ti)O_3/ZrO_2/SiO_2$ stacks for piezoelectric microactuators, Thin Solid Films 510 (January) (2006) 213–221.